ENGINEERING

Zebra-inspired stretchable, biodegradable radiation modulator for all-day sustainable energy harvesters

Won Bae Han[1]†, Se-Yeon Heo[2]†, Donghak Kim[1,3]†, Seung Min Yang[1], Gwan-Jin Ko[1], Gil Ju Lee[4], Dong-Je Kim[1], Kaveti Rajaram[1], Joong Hoon Lee[1], Jeong-Woong Shin[1], Tae-Min Jang[1], Sungkeun Han[1], Heeseok Kang[1], Jun Hyeon Lim[1], Do Hyeon Kim[2], Soo Hyun Kim[1,3], Young Min Song[2,5]*, Suk-Won Hwang[1,3,6]*

Recent advances in passive radiative cooling systems describe a variety of strategies to enhance cooling efficiency, while the integration of such technology with a bioinspired design using biodegradable materials can offer a research opportunity to generate energy in a sustainable manner, favorable for the temperature/climate system of the planet. Here, we introduce stretchable and ecoresorbable radiative cooling/heating systems engineered with zebra stripe–like patterns that enable the generation of a large in-plane temperature gradient for thermoelectric generation. A comprehensive study of materials with theoretical evaluations validates the ability to accomplish the target performances even under external mechanical strains, while all systems eventually disappear under physiological conditions. Use of the zebra print for selective radiative heating demonstrates an unexpected level of temperature difference compared to use of radiative cooling emitters alone, which enables producing energy through resorbable silicon-based thermoelectric devices. The overall result suggests the potential of scalable, ecofriendly renewable energy systems.

INTRODUCTION

Many research efforts have been introduced to address global climate change and environmental issues, particularly a passive cooling technology, which can dissipate Earth's heat by thermal radiation to the cold outer space, suggesting practical applications, such as personal thermal management (*1*) and reduction of cooling energy consumption in residential and industrial areas (*2*–*4*). Such possible solutions highlighted fundamental aspects with materials options, including thin-film stacks (*5*–*7*), inorganic-organic hybrid films (*8*, *9*), and porous polymer membranes (*10*–*12*) to meet the optical requirement for all-day radiative cooling, i.e., high reflectivity in the solar spectrum [wavelength (λ), 0.3 to 2.5 μm] and high emissivity in the long-wave infrared region (LWIR; λ, ~8 to 13 μm). Although the results accomplished technological advances in a diverse range of research realms, there has been little consideration for systems that are critically linked to the sustainability of ecosystems by alleviating the environmental and economic challenges arising from the notable increase in end-of-life electronic waste and disposal. In this context, management and reduction of wastes can be realized via bioresorbable elements whose degradable and nontoxic behaviors in biological environments have already been verified by various reports associated with implantable biomedical electronics (*13*–*16*), wearable electronic systems (*17*, *18*), drug carriers (*19*, *20*), and tissue scaffolds (*21*, *22*). Because the chemical bonds and tunable nano/microstructures of polymers are known to absorb LWIR light and reflect the solar spectrum effectively (*10*), fibrous biodegradable polymer membranes may represent an attractive starting point.

Direct conversion of temperature gradients to thermoelectric potentials offers an opportunity to generate electricity as off-grid or standalone renewable energy, as demonstrated in a previous attempt (*23*). Typical schemes involve a selective emitter with high IR emissivity to form the cool region at the top of a thermoelectric generator (TEG), while the bottom side is heated by ambient surroundings or solar energy with extended structures or vice versa (*24*–*26*). Although the strategies that exploited a combined use of solar power with radiative cooling improved the temperature gradients, complex and inefficient out-of-plane configurations in a very rigid and bulky format restrict degrees of freedom or scalability to build sophisticated, future-oriented systems via integration with other components or waste a large area because of the modified geometries for solar heating/cooling.

In the following, we present a set of materials, design strategies, and modeling tools for a biologically degradable and benign, mechanically soft thermoelectric harvester based on a radiative cooling/heating system. The formation of black and white stripes of living zebras enables the creation of a large in-plane thermal gradient, offering a highly competitive route to scalable, integrable, and sustainable energy systems over those available with conventional out-of-plane systems.

[1]KU-KIST Graduate School of Converging Science and Technology, Korea University, 145 Anam-ro, Seongbuk-gu, Seoul 02841, Republic of Korea. [2]School of Electrical Engineering and Computer Science, Gwangju Institute of Science and Technology (GIST), 123 Cheomdangwagi-ro, Buk-gu, Gwangju 61005, Republic of Korea. [3]Center for Biomaterials, Biomedical Research Institute, Korea Institute of Science and Technology (KIST), 5 Hwarang-ro 14-gil, Seongbuk-gu, Seoul 02792, Republic of Korea. [4]Department of Electronics Engineering, Pusan National University, 2 Busandaehak-ro, Geumjeong-gu, Busan 46241, Republic of Korea. [5]Artificial Intelligence (AI) Graduate School, Gwangju Institute of Science and Technology (GIST), 123 Cheomdangwagi-ro, Buk-gu, Gwangju 61005, Republic of Korea. [6]Department of Integrative Energy Engineering, Korea University, 145 Anam-ro, Seongbuk-gu, Seoul 02841, Republic of Korea.
*Corresponding author. Email: ymsong@gist.ac.kr (Y.M.S.); dupong76@korea.ac.kr (S.-W.H.)
†These authors contributed equally to this work.

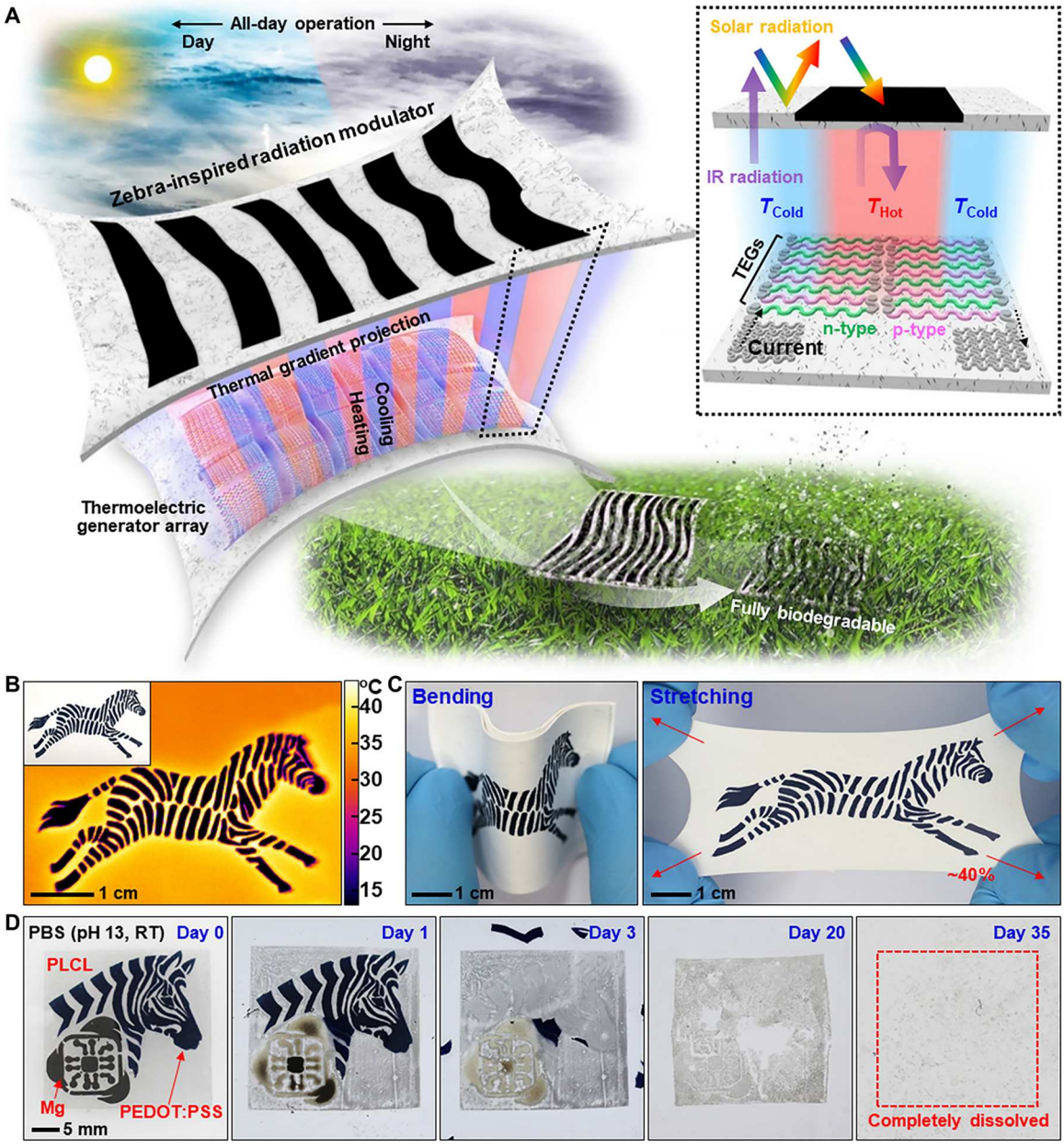

Fig. 1. Zebra-inspired modulation of radiative energy for all-day energy scavenging. (**A**) Schematic illustration of a biodegradable, stretchable energy-harvesting system consisting of a PLCL microfiber membrane coated with patterns of PEDOT:PSS as radiative cooling/heating components for all-day thermal gradients and n- and p-doped Si NM arrays for thermoelectric generation. (**B**) IR and corresponding digital photographs (inset) of a PLCL membrane with PEDOT:PSS-based zebra print. (**C**) Optical images of a zebra-patterned device upon bending (left) and stretching (right). (**D**) A collection of dissolution images of a representative device at several stages, constructed with PLCL/PEDOT:PSS membrane and Mg film, in PBS (pH 13) at room temperature (RT) (under an accelerated condition), although dissolution rate can be extended over a year under the biological condition. Photo credit: Won Bae Han and Seung Min Yang, Korea University.

RESULTS

Ecoresorbable, sustainable energy scavenging system

Figure 1A illustrates a sustainable power scavenger using a radiation modulating cooler/heater inspired by zebra stripes (top layer), coupled with TEGs (bottom layer). We exploited a stretchable and biodegradable poly(L-lactide-co-ε-caprolactone) (PLCL)–based white fibrous membrane with strong solar reflection and IR emission, partially coated with conductive, black poly(3,4-ethylenedioxythiophene):poly(styrenesulfonate) (PEDOT:PSS) with high solar absorption and IR reflection, yielding apparent, alternate hot and cold regions in a planar geometry as black and white stripes of zebras. Arrays of doped p- and n-type silicon nanomembranes (Si NMs) with a serpentine configuration connected in series via dissolvable magnesium (Mg) interconnects on the bottom layer experienced a large temperature gradient, which caused charge carriers in the Si NMs to diffuse from hot to cold regions, enabling the generation of thermoelectric potential. IR images of a zebra-patterned device in Fig. 1B clearly verified the key role of the proposed

design: The higher the surface emission, the higher the surface temperature in the thermogram (*27*). In other words, PLCL regions were effectively cooled by emitting heat into space, while conductive PEDOT:PSS-coated regions were heated by hampering the thermal emission during the day and night. This polymeric membrane–based energy harvester has mechanically reversible stability under external stimuli, such as bending and stretching, due to the intrinsic elasticity (PLCL) (*28*) as well as materials and structural engineering (i.e., addition of a plasticizer to PEDOT:PSS and serpentine layouts of inorganic Si NMs and Mg) (Fig. 1C). Figure 1D exhibits the temporal degradation behavior of a representative device constructed by depositing PEDOT:PSS and Mg layers on a porous PLCL membrane during immersion in a phosphate-buffered saline (PBS; pH 13) at room temperature. The Mg layer rapidly dissolved via hydrolysis [$Mg + 2H_2O \rightarrow Mg(OH)_2 + H_2$] (*29*), while the PEDOT:PSS layer gradually broke into small fragments as the PLCL membrane degraded through the cleavage of polymer backbones (*30*, *31*). Then, the device entirely disappeared after 35 days without remaining by-products harmful to the natural environment.

Mechanical/biochemical properties of biodegradable polymer membranes

Electrospinning of a range of synthetic biodegradable polymers [PLCL (molecular structure in fig. S1), poly(ε-caprolactone) (PCL), and poly(lactic acid) (PLA)] with different concentrations (5 to 20%) produced white polymeric membranes with fibers and pores of various sizes depending on the viscosity of polymer solutions (fig. S2). Figure 2A demonstrates a large-scale PLCL membrane (L-lactide to ε-caprolactone ratio of 50:50) with an exceptional elongation of more than ~1500%, with an image at the undeformed state and its magnified view of microstructure in the inset. Although PCL (10%) and PLA (10%) membranes also exhibited elasticity, they experienced irreversible deformation (Fig. 2B). The PLCL (5%) membrane, however, showed reversible, stable stretchability with negligible hysteresis after 1000 cyclic tests at a linear strain of 40% (Fig. 2C). Figure 2D displays calculated toughnesses of the respective membranes; in particular, a resilient and durable PLCL (5%) membrane could lift up an object ~33,000 times heavier (5000 g) than the membrane weight (~0.15 g). Other mechanical and physical properties, including water contact angles and vapor permeability, appear in fig. S3 and table S1. All the polymer membranes were hydrophobic (~120°C) and breathable (~0.1 g/cm^2 per day) due to hierarchically interconnected pores, which prevent or minimize any possible discomfort and sweat accumulation when used in on-skin applications (*11*). Figure 2E compares dissolution behaviors of degradable polymeric membranes in PBS under accelerated conditions (pH 13 at 50°C). The degradation rate of PCL membranes was faster than the other ones because the number of hydrophobic $-CH_2$ moieties in repeating units of PCL is higher than that of PLA (*32*). As the temperature and pH of the solution increased, the hydrolysis of ester bonds in polymers accelerated, resulting in rapid dissolution behaviors of the PLCL membranes (Fig. 2, F and G), which is in good agreement with the previous results (*33*).

Radiative cooling performance of PLCL membranes

As the nano- and microsized pores in polymeric media strongly interact with the solar spectrum (*34*), experimental and theoretical investigations of PLCL membranes can provide optimized conditions for desirable cooling efficiency. Figure 3A shows cross-sectional views of scanning electron microscopy (SEM) and binary images of PLCL membranes with different concentrations. The fiber densities were 54, 53, and 54% for PLCL (5, 10, and 15%) membranes, whose mean diameters were 1.7, 2.9, and 4.5 μm, respectively. Using this information, we constructed computational models of the PLCL membranes and conducted finite-difference time-domain (FDTD) simulations (Fig. 3B). When an electromagnetic wave with a wavelength of 500 nm (i.e., the peak wavelength of the solar energy) was incident on the PLCL models, the intensity of the electric field gradually decayed from the top surface. The amplitude of the electric field reached zero at different distances for PLCL (5, 10, and 15%) membranes, all of which were much shorter than the membrane thickness (500 μm) used for our experiments. In particular, the PLCL (5%) membrane showed the shortest distance (<~25 μm) for light to disappear across the solar spectrum (figs. S4 and S5), indicating the most efficient solar reflectance. Figure 3C presents distributions of interfiber distance (pore diameter), *D*, of the PLCL (5%) membrane before (i.e., 0% stretching) and after 100% stretching. The original distribution profile (*D*, 0.5 to ~4 μm) with an average value of ~0.8 μm was almost maintained after the 100% stretching, which enabled the PLCL (5%) membrane to scatter the sunlight even in deformation modes effectively. This is because the broad distributions of the interfiber distance covered the whole solar spectrum, as confirmed in the scattering efficiency simulation (Fig. 3D). Consequently, spectral measurements in Fig. 3E and fig. S6 revealed that the membrane provided identical solar reflectance (>95%) regardless of the applied strains. The theoretical estimation based on the experimental values exhibited a maximum cooling power of 136 W/m^2 for the PLCL (5%), comparable to those of state-of-the-art devices (Fig. 3F, fig. S7, note S5, and table S2) (*35*, *36*). Outdoor field tests for four different days showed subambient cooling of PLCL membranes with all concentrations (Fig. 3G and fig. S8), with a temperature decrease of up to ~7.3°C under a peak solar intensity of 1000 W/m^2. Furthermore, PLCL (5%) membranes retained cooling performance even under 50 and 100% stretching (Fig. 3H, figs. S9 and S10, and note S6), consistent with the analysis in Fig. 3F.

All-day thermoelectric generation through zebra-inspired radiation modulator

The resulting thermal management via radiative cooling can be explored in versatile research directions through slight modifications to the polymeric membrane and/or integration with electronic components. Figure 4A illustrates a stretchable, scalable, sustainable energy-harvesting system consisting of a radiation modulator (top layer) and TEG (bottom layer). Zebra-like patterns of conductive PEDOT:PSS on a passive radiative cooler produced alternate regions of solar absorption and reflection (IR reflection and emission, respectively), which created extreme "in-plane" temperature gradients. Such sufficient heat flux was transferred to the thermoelectric modules in Fig. 4B. Here, the magnitude of thermoelectric power depends on efficiencies of a radiative heater (i.e., the solar absorption and IR reflection characteristics) and a cooler. Figure 4C and fig. S11 exhibit the capability of several candidate materials, where PEDOT:PSS and tungsten (W) foil satisfied both high absorptivity in the solar spectrum [equal to high solar emissivity according to Kirchhoff's law of radiation (*6*)] and low sky-window emissivity (high IR reflectance). Any material that is optically

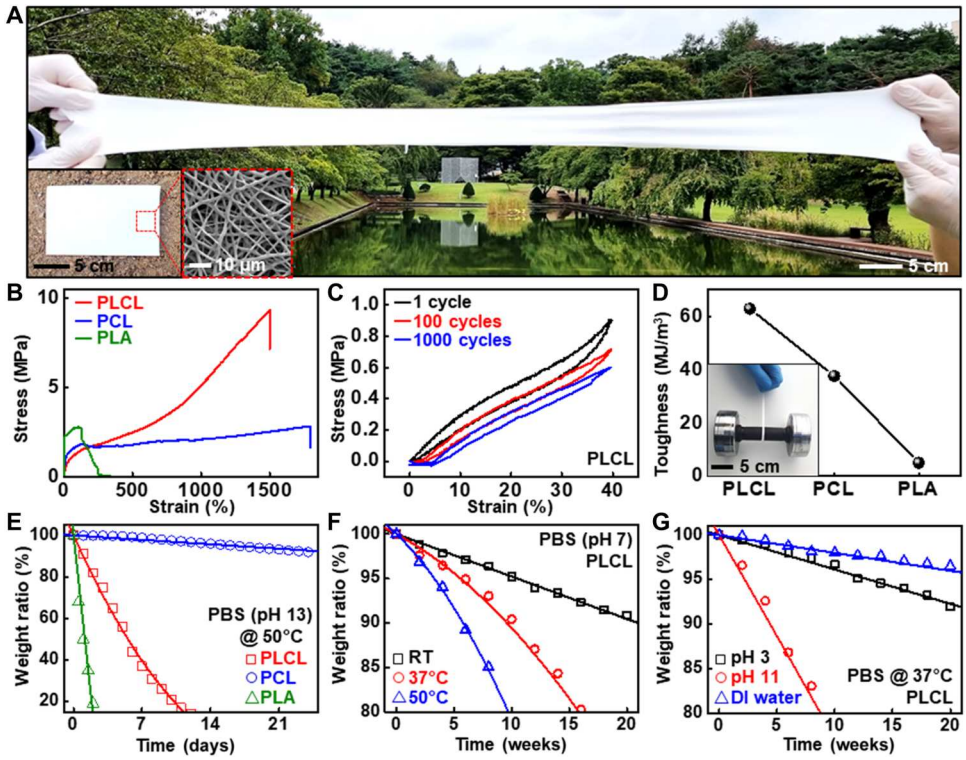

Fig. 2. Mechanical and biochemical properties of biodegradable polymer-based microfiber membranes as radiative cooling textiles. (**A**) Superelastic response of a large-scale PLCL membrane with a linear strain of ~700% and an original state with its microstructure (inset). (**B**) Stress-strain curves of different biodegradable membranes based on PLCL, PCL, and PLA. (**C**) Cyclic mechanical behavior of a PLCL membrane under a uniaxial tensile strain of 40%. (**D**) Toughness of PLCL, PCL, and PLA membranes and a photograph of a PLCL membrane (thickness, 500 μm; width, 5 mm) holding a dumbbell (~5 kg) in the inset. (**E**) Time-dependent changes in weight ratios of PLCL, PCL, and PLA membranes in PBS (pH 13) at 50°C. (**F** and **G**) Effects of temperature (F) and pH (G) on dissolution rates of PLCL membranes in PBS. Photo credit: Won Bae Han and Donghak Kim, Korea University.

dark and electrically conductive can substitute for PEDOT:PSS and W foil. However, a typical black ink obtained high solar absorption but poor IR reflectance (fig. S12), because of its nonconductive nature, as explained by the Hagen-Rubens equation: The reflectance of material $= 1 - 4\sqrt{\nu\pi\varepsilon_0/\sigma}$, where ν, ε_0, and σ are the light frequency, the vacuum permittivity, and the conductivity of material, respectively (*37*). PEDOT:PSS generated a relatively large temperature difference (ΔT, 19°C) during the daytime, while W foil was found to be effective (ΔT, 0.35°C) in the nighttime (Fig. 4D). The calculated heating/cooling powers of those materials and cooling behaviors at nighttime appear in fig. S13. The temperature slope can be further improved by increasing the pattern size due to reduction of the parasitic heat flow (conduction/convection), which confirmed that a pattern size of 30 mm by 30 mm yielded a maximum ΔT of 24°C (daytime) and 2.8°C (nighttime) (Fig. 4E). The overall experimental setup appears in fig. S14.

The formation of cooling/heating in the horizontal direction can facilitate integration with monolithic, large-scale thermoelectric components. We prepared bioresorbable, scalable Si NMs as well as high-performance bismuth telluride (Bi-Te) as TEGs and examined several key characteristics. Figure 4F shows output voltages of both TEGs at various steady temperature differences. The results correspond to the Seebeck coefficients of 223 and 197 μV/K for p- and n-type Bi-Te, and 68 and 65 μV/K for p- and n-type Si NMs, which are consistent with previously reported values (*38*, *39*). The Seebeck coefficient (S) and power factors relying on silicon doping conditions and test setup appear in fig. S15. Single Bi-Te module (a pair of p- and n-type legs) yielded an open-circuit voltage (V_{oc}) of ~8.4 mV and a maximum output power density of ~270 mW/m^2 at a temperature difference of 20 K, while 20 of each p- and n-type Si NM leg generated ~52 mV (V_{oc}) and ~0.04 mW/m^2 (power density) under the same conditions (Fig. 4G; detailed layouts in fig. S16).

To demonstrate a proof of concept, we measured real-time outdoor power generation of energy-harvesting systems with the radiation modulator for a day (Fig. 4H and fig. S17). A device with the Bi-Te array harvested an output power density of ~0.003 to 40 mW/m^2 as a function of solar irradiance, which is comparable to output performances of previously reported stretchable and flexible TEGs (*40*, *41*). On the other hand, the ultrathin silicon-based system produced a maximum output power density of ~0.006 mW/m^2, whose low-energy level was ascribed to the low thermoelectric figure of merit of Si ($zT > 0.001$ at 300 K), and can be further improved via forms of nanowires/fibers with low thermal conductivity (*42*, *43*). Detailed plots of power density appear in fig. S18. The system has excellent mechanical properties, capable of retaining the original performances against axial/biaxial stretching up to 25% and repeated loading of 25% strain for 1000 cycles (fig. S19). So far, none of the radiative cooling–based energy harvesters have simultaneously achieved stretchability, biodegradability, and scalability while

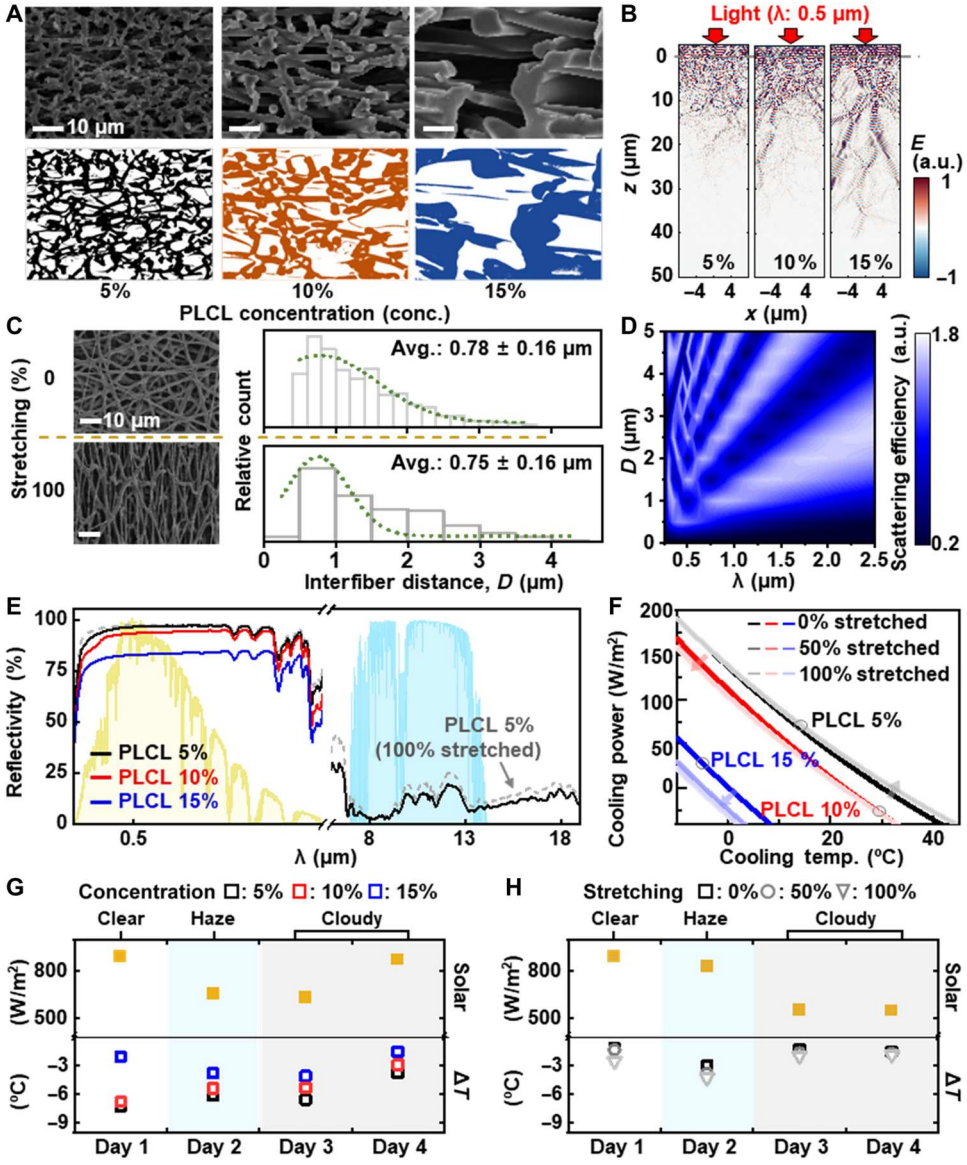

Fig. 3. Optical features of PLCL membranes with different concentrations and stretching ratios. (**A**) Cross-sectional views of SEM and binary images of PLCL membranes with different concentrations (5, 10, and 15%). (**B**) Electric field distributions of computational models for fibers with diameters of 1.7 μm (5% concentration), 2.9 μm (10% concentration), and 4.5 μm (15% concentration) at a density of ~54%. (**C**) SEM images and pore size distributions of PLCL membranes (5%) before (top) and after (bottom) 100% stretching. (**D**) Scattering efficiency of circular vacancy in PLCL membrane. (**E**) Reflectivity of PLCL membranes with 5, 10, and 15% concentrations, and a 100% stretched PLCL membrane (5% concentration) is shown in gray dashed line. (**F**) Calculated cooling temperature and power of PLCL membranes at various concentrations (5 to 15%) and mechanical strains (0 to 100%). (**G**) Average solar intensity and cooling temperature (ΔT) at 5, 10, and 15% concentrations of PLCL membranes. (**H**) Average solar intensity and cooling temperature (ΔT) of PLCL membranes at applied strains of 0, 50, and 100% (5% concentration). Photo credit: Se-Yeon Heo, GIST.

generating large temperature gradients throughout the day (table S3), paving the way toward a new type of sustainable energy source.

DISCUSSION

The concepts, materials, and system design reported here propose an innovative strategy to construct a stretchable and ecoresorbable radiative cooling/heating platform for all-day energy harvesting. Along with experimental and theoretical evaluations, a facile method for fabricating a fibrous membrane could be applied to other polymers to create efficient and biodegradable radiative cooling systems. The design of a zebra stripe–like radiation-modulating pattern for radiative cooling and solar heating produced a large in-plane temperature gradient, which outperformed the previously reported devices based on radiative cooling alone. Coupled with TEG modules, the proposed system could generate energy throughout the day without performance deterioration, even under external strains, highlighting the potential applicability of sustainable and renewable energy harvesters.

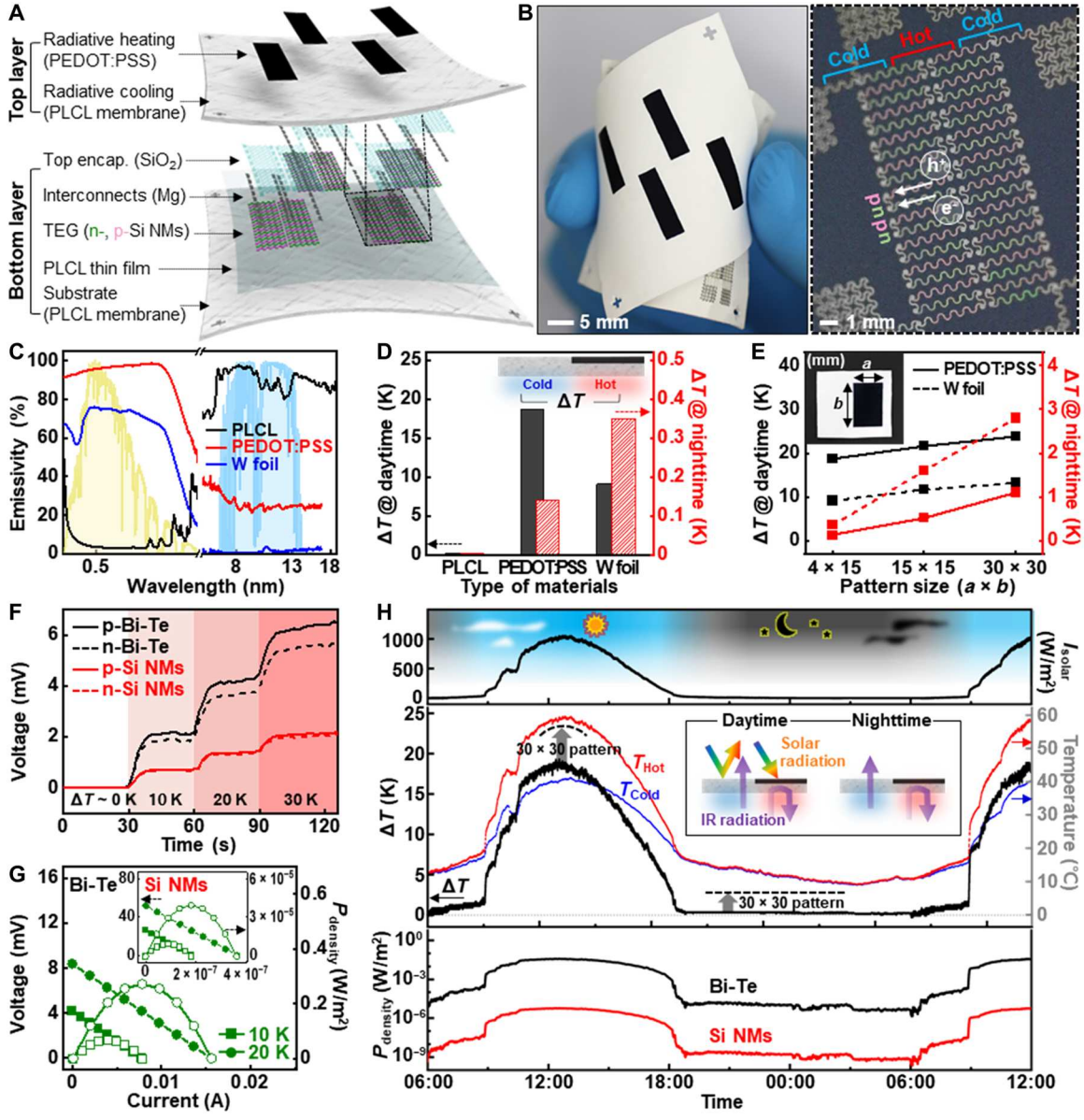

Fig. 4. All-day energy harvesting enabled by the combination of radiation modulation and thermoelectric generation. (**A**) Schematic exploded view of a stretchable, biodegradable energy harvester, with layers of zebra-inspired radiation modulator and in-plane TEG. (**B**) Photograph of the energy harvester (left) and arrays of n- and p-type Si NM-based TEGs (right). (**C**) Spectral emissivity of PLCL membranes, partially coated with PEDOT:PSS and W foil for radiative heating, with normalized ASTM G173 global solar spectrum (0.3 to 2.5 μm) and the LWIR (8 to 13 μm) atmospheric transparency window shaded as the yellow and blue regions, respectively. (**D**) Experimentally measured temperature differences between hot and cold regions (ΔT) at daytime (1000 W/m^2) and nighttime (0 W/m^2) as a function of types of radiative heating materials. (**E**) Effect of radiative heating pattern size on ΔT at daytime and nighttime, and an optical image of PLCL membrane coated with PEDOT:PSS (inset). (**F**) Generation of thermoelectric voltages of p- and n-type bismuth telluride (Bi-Te) and Si NM TEG legs at various steady temperature differences. (**G**) Power output characteristics of the TEG modules (a pair of n- and p-type Bi-Te; 20 of each n- and p-type Si NMs) at ΔT of 10 and 20 K. (**H**) Temporal measurements of solar irradiance, ΔT, and power density for a day, showing all-day possible energy generation (maximum power densities with Bi-Te at daytime and nighttime, ~40 and ~0.003 mW/m^2). A fully biodegradable device based on Si NMs harvested power densities of up to 0.006 mW/m^2. Using a larger radiative heating pattern (30 × 30) can produce a higher ΔT to increase the output power as confirmed in (E). Photo credit: Won Bae Han, Korea University.

MATERIALS AND METHODS

Fabrication of biodegradable microfiber membranes

The PLCL solutions were prepared by dissolving PLCL polymer (M_n, 130k) in 1,1,1,3,3,3,-hexafluoro-2-propanol (Tokyo Chemical Industry, Japan) at concentrations of 5, 10, and 15% (w/v) and mixed overnight. These solutions were loaded into a 12-ml syringe with a 21-gauge needle and used for electrospinning at a high voltage of 15 kV using a single-syringe infusion pump (NNC-ESR100RD, NanoNC, Korea). The flow rate of the syringe pump was fixed at 0.6 ml hour^{-1}, a stainless steel mandrel as a collector was rotated at a speed of 90 rpm, and the distance between the collector and the needle tip was 13 cm. The final thickness of PLCL

membranes was ~500 μm. PCL and PLA membranes were also fabricated in the same method using PCL (M_n, 80k; Sigma-Aldrich, USA) and PLA (M_w, 75k to 120k; Sigma-Aldrich, USA) solutions with different concentrations of 10, 15, and 20% (w/v). The viscosity of the prepared solutions was measured using a viscometer (Viscotek Y501, Houston MJ Associates, USA).

Electromagnetic field and scattering efficiency simulation

SEM (S-4700, Hitachi Hi-Tech, Japan) was used to characterize the surface morphology of PLCL membranes. The fiber densities and pore distributions were analyzed using ImageJ software. We kept an auto-threshold condition for all SEM images. Using the average pore size and ratio obtained from the SEM analysis, random fiber structure models were developed using MATLAB R2018A (MathWorks Inc., USA) for PLCL membranes with varying concentrations. These models were then imported into commercial software (Rsoft, FullWAVE, RSoft Design Group, Synopsys, USA) for further analysis. After that, a two-dimensional (2D) FDTD simulation was used to investigate the effect of fiber structures on the dynamics of electromagnetic fields in PLCL membranes. A plane wave in the wavelength range of 200 to 2500 nm for the solar spectrum is launched at a distance of 5 μm from the surface of the generated random air void structures to simulate the penetration depth of light into the structure. The refractive indices of PLCL were set to a constant value of 1.5.

Scattering cross sections of interfiber distance (0 to 5 μm) in PLCL membranes were simulated using a 2D FDTD simulation. Scattering cross sections of circles, assumed to be interfiber distance, were calculated with different diameters of 1.7, 2.9, and 4.5 μm. For 2D FDTD simulations, Maxwell's equations are separable, and transverse magnetic (TM) simulation was chosen. Because the calculation of TM oscillates with respect to the radius, 2D simulation results were close to the 3D calculation.

Outdoor cooling performance measurement

Measurement of outdoor cooling performance of PLCL membranes before and after stretching was conducted at the Gwangju Institute of Science and Technology (GIST; 35° 13′ 36.5″ N, 126° 50′ 24.0″ E), using a custom-made experimental setup as shown in fig. S8. Briefly, the setup consisted of an acrylic chamber covered by low-density polyethylene film as a convection shield, Styrofoam as a conduction shield, and ambient sensor that is covered by aluminum (Al) foil to prevent overheating by solar irradiance. A pyranometer (CMP6, Kipp & Zonen, Netherlands) was placed beside the setup to measure solar irradiance. Temperature sensors (ST-50, RKC Instrument Inc., Japan) were connected to a data logger (OM-CP-OCTRTD, Omega Engineering, USA) to record the real-time temperature of PLCL membranes and ambient air. For stretching samples, we used a custom-made stretching zig composed of a polycarbonate body and an Al holder (fig. S9). PLCL membranes were located on the body coated with Al foil and enhanced specular reflector film (3M ESR). The setup was placed on a wood table at a height of 1 m to avoid any heating from the ground.

Fabrication and characterization of radiative cooling/heating patterns

All experiments were conducted on the rooftop of the R&D Center at Korea University (37°35′ N, 127°01′ E) in late March when it was almost cloudless and windless. The PLCL membranes with radiative heating patterns were fabricated by depositing 3 ml of black ink (Midnight Black, Chefmaster, USA) or PEDOT:PSS aqueous solution (Clevios PH1000, Heraeus, Germany) mixed with 150 μl of dimethyl sulfoxide and 30 μl of lithium bis(trifluoromethanesulfonyl)imide (LiTFSI) (Sigma-Aldrich, USA) on an oxygen plasma–treated PLCL membrane through a polydimethylsiloxane (PDMS) mask using a spray coater (BBM-P001, Beetlebug, South Korea), followed by drying on a hot plate at 50°C for 12 hours or attaching W foil patterned using a laser cutter (Epilog Legend Helix, Epilog laser, USA) on an oxygen plasma–treated PLCL membrane using an adhesive (Loctite 401, Henkel, Germany). Then, the samples were mounted on the setup for radiative cooling performance measurements with minor modification (fig. S14). The temperature difference between hot and cold sides (ΔT) was monitored using K-type thermocouples connected to a multichannel data logger (resolution, ±0.1°C; RDXL6SD-USB, OMEGA, USA) under the solar irradiance of 1000 W/m^2 (daytime) and 0 W/m^2 (nighttime).

Fabrication of Si NMs and Bi-Te–based energy harvesters

Detailed layouts for the device appear in Fig. 4A and fig. S16. The top layer for radiation modulation was fabricated as described above. The fabrication of the bottom layer for thermoelectric generation began with thermal growth (1100°C, 30 min) of silicon dioxide (SiO_2; 100 nm) as masks for doping on a silicon-on-insulator (p-type, top Si 300 nm; SOITEC, France) wafer. Photolithography using a photoresist (S1805, MicroChem, USA) and subsequent wet etching in a buffered oxide etchant (J. T. Baker, USA) defined openings in the SiO_2 for solid-state diffusion doping. High-temperature annealing with boron (1100°C, 15 min) and phosphorus (950°C, 5 min) yielded p- and n-type regions. Here, individual SiO_2 masks were used for each dopant type. Removal of the buried oxide by wet etching with 49% of hydrofluoric acid released the p- and n-type Si NM array from the wafer, allowing its retrieval by a slab of PDMS and transfer printing onto a bilayer of diluted polyimide (D-PI; Sigma-Aldrich, USA)/poly(methylmethacrylate) (PMMA; Microchem, USA) spin-coated on a silicon handling wafer. Reactive ion etching (RIE) with sulfur hexafluoride enabled the isolation of the Si NMs into a serpentine layout. A pattern of physically deposited Mg (1 μm) served as interconnects and electrodes. A thin layer of SiO_2 encapsulated the device without openings for contact pads, and casting a layer of D-PI on the SiO_2 completed the stack. Patterned dry etching removed certain regions of the stack to define mesh structure. Immersion in acetone dissolved the PMMA to release the device from the handling wafer, allowing its retrieval using a PDMS stamp. After eliminating the exposed D-PI layer by oxygen RIE, transfer printing delivered the device onto a PLCL sheet (50 μm). The bottom side of the PLCL sheet was treated with oxygen plasma (50 W, 30 standard cubic centimeters per minute, 30 mtorr, 60 s) and bonded to an oxygen plasma–treated PLCL microfiber membrane. Removal of the top D-PI layer by oxygen RIE completed the process. For the Bi-Te–based bottom layer, p-type $Bi_{0.5}Sb_{1.5}Te_3$ and n-type $Bi_2Te_{2.7}Se_{0.3}$ ingots (Wuhan Tuocai Technology, China) were cut into 400-μm-thick sheets by electrical discharge machining, polished, deposited with copper (0.5 μm) as interconnects and electrodes by sputtering, and attached to a PLCL microfiber membrane using an adhesive. The aligned assembly of the prepared top and bottom (Si NMs or Bi-Te) layers completed the energy harvesters.

Demonstration of all-day energy-harvesting performance

Thermoelectric output power and ΔT were recorded for the energy-harvesting device with PEDOT:PSS radiative heating pattern (size, 4 × 15 mm^2) for a day in a similar manner to the characterization of radiative heating materials. Areal power density ($P_{density}$) was calculated by the equation $P_{density} = V_{oc}^2/(4 \times R_{module} \times A_{module})$, where V_{oc}, R_{module}, and A_{module} were the measured open-circuit voltage, resistance, and the area of single Bi-TE (or Si NMs) TEG module, respectively.

Supplementary Materials

This PDF file includes:

Notes S1 to S8
Figs. S1 to S19
Tables S1 to S3
References

REFERENCES AND NOTES

1. B. Zhu, W. Li, Q. Zhang, D. Li, X. Liu, Y. Wang, N. Xu, Z. Wu, J. Li, X. Li, P. B. Catrysse, W. Xu, S. Fan, J. Zhu, Subambient daytime radiative cooling textile based on nanoprocessed silk. *Nat. Nanotechnol.* **16**, 1342–1348 (2021).
2. T. Li, Y. Zhai, S. He, W. Gan, Z. Wei, M. Heidarinejad, D. Dalgo, R. Mi, X. Zhao, J. Song, J. Dai, C. Chen, A. Aili, A. Vellore, A. Martini, R. Yang, J. Srebric, X. Yin, L. Hu, A radiative cooling structural material. *Science* **364**, 760–763 (2019).
3. S. Y. Heo, G. J. Lee, D. H. Kim, Y. J. Kim, S. Ishii, M. S. Kim, T. J. Seok, B. J. Lee, H. Lee, Y. M. Song, A *Janus* emitter for passive heat release from enclosures. *Sci. Adv.* **6**, eabb1906 (2020).
4. J.-W. Cho, S.-S. Yoon, E.-J. Lee, S.-K. Kim, Anti-greenhouse effect via regulation of surface emissivity. *IEEE Photonics J.* **14**, 1–7 (2022).
5. G. J. Lee, Y. J. Kim, H. M. Kim, Y. J. Yoo, Y. M. Song, Colored, daytime radiative coolers with thin-film resonators for aesthetic purposes. *Adv. Opt. Mater.* **6**, 1800707 (2018).
6. A. P. Raman, M. A. Anoma, L. Zhu, E. Rephaeli, S. Fan, Passive radiative cooling below ambient air temperature under direct sunlight. *Nature* **515**, 540–544 (2014).
7. J.-W. Cho, E.-J. Lee, S.-K. Kim, Full-color solar-heat-resistant films based on nanometer optical coatings. *Nano Lett.* **22**, 380–388 (2022).
8. Y. Zhai, Y. Ma, S. N. David, D. Zhao, R. Lou, G. Tan, R. Yang, X. Yin, Scalable-manufactured randomized glass-polymer hybrid metamaterial for daytime radiative cooling. *Science* **355**, 1062–1066 (2017).
9. L. Zhou, H. Song, J. Liang, M. Singer, M. Zhou, E. Stegenburgs, N. Zhang, C. Xu, T. Ng, Z. Yu, B. Ooi, Q. Gan, A polydimethylsiloxane-coated metal structure for all-day radiative cooling. *Nat. Sustain.* **2**, 718–724 (2019).
10. J. Mandal, Y. Fu, A. C. Overvig, M. Jia, K. Sun, N. N. Shi, H. Zhou, X. Xiao, N. Yu, Y. Yang, Hierarchically porous polymer coatings for highly efficient passive daytime radiative cooling. *Science* **362**, 315–319 (2018).
11. Y. Peng, J. Chen, A. Y. Song, P. B. Catrysse, P. C. Hsu, L. Cai, B. Liu, Y. Zhu, G. Zhou, D. S. Wu, H. R. Lee, S. Fan, Y. Cui, Nanoporous polyethylene microfibres for large-scale radiative cooling fabric. *Nat. Sustain.* **1**, 105–112 (2018).
12. M. H. Kang, G. J. Lee, J. H. Lee, M. S. Kim, Z. Yan, J.-W. Jeong, K.-I. Jang, Y. M. Song, Outdoor-useable, wireless/battery-free patch-type tissue oximeter with radiative cooling. *Adv. Sci.* **8**, 2004885 (2021).
13. W. B. Han, J. H. Lee, J. W. Shin, S.-W. Hwang, Advanced materials and systems for biodegradable, transient electronics. *Adv. Mater.* **32**, e2002211 (2020).
14. S. K. Kang, R. K. J. Murphy, S. W. Hwang, S. M. Lee, D. V. Harburg, N. A. Krueger, J. Shin, P. Gamble, H. Cheng, S. Yu, Z. Liu, J. G. McCall, M. Stephen, H. Ying, J. Kim, G. Park, R. C. Webb, C. H. Lee, S. Chung, D. S. Wie, A. D. Gujar, B. Vemulapalli, A. H. Kim, K. M. Lee, J. Cheng, Y. Huang, S. H. Lee, P. V. Braun, W. Z. Ray, J. A. Rogers, Bioresorbable silicon electronic sensors for the brain. *Nature* **530**, 71–76 (2016).
15. J. Lee, H. R. Cho, G. D. Cha, H. Seo, S. Lee, C. K. Park, J. W. Kim, S. Qiao, L. Wang, D. Kang, T. Kang, T. Ichikawa, J. Kim, H. Lee, W. Lee, S. Kim, S. T. Lee, N. Lu, T. Hyeon, S. H. Choi, D. H. Kim, Flexible, sticky, and biodegradable wireless device for drug delivery to brain tumors. *Nat. Commun.* **10**, 5205 (2019).
16. S. M. Yang, J. H. Shim, H.-U. Cho, T.-M. Jang, G.-J. Ko, J. Shim, T. H. Kim, J. Zhu, S. Park, Y. S. Kim, S.-Y. Joung, J. C. Choe, J.-W. Shin, J. H. Lee, Y. M. Kang, H. Cheng, Y. Jung, C.-H. Lee, D. P. Jang, S.-W. Hwang, Hetero-integration of silicon nanomembranes with 2D materials for bioresorbable, wireless neurochemical system. *Adv. Mater.* **34**, 2108203 (2022).
17. M. Baumgartner, F. Hartmann, M. Drack, D. Preninger, D. Wirthl, R. Gerstmayr, L. Lehner, G. Mao, R. Pruckner, S. Demchyshyn, L. Reiter, M. Strobel, T. Stockinger, D. Schiller, S. Kimeswenger, F. Greibich, G. Buchberger, E. Bradt, S. Hild, S. Bauer, M. Kaltenbrunner, Resilient yet entirely degradable gelatin-based biogels for soft robots and electronics. *Nat. Mater.* **19**, 1102–1109 (2020).
18. M. Zarei, G. Lee, S. G. Lee, K. Cho, Advances in biodegradable electronic skin: Material progress and recent applications in sensing, robotics, and human–machine interfaces. *Adv. Mater.* , 2203193 (2022).
19. J. Nicolas, S. Mura, D. Brambilla, N. Mackiewicz, P. Couvreur, Design, functionalization strategies and biomedical applications of targeted biodegradable/biocompatible polymer-based nanocarriers for drug delivery. *Chem. Soc. Rev.* **42**, 1147–1235 (2013).
20. Y. Arun, R. Ghosh, A. J. Domb, Biodegradable hydrophobic injectable polymers for drug delivery and regenerative medicine. *Adv. Funct. Mater.* **31**, 2010284 (2021).
21. H. S. Lee, E. Y. Jeon, J. J. Nam, J. H. Park, I. C. Choi, S. H. Kim, J. J. Chung, K. Lee, J. W. Park, Y. Jung, Development of a regenerative porous PLCL nerve guidance conduit with swellable hydrogel-based microgrooved surface pattern via 3D printing. *Acta Biomater.* **141**, 219–232 (2022).
22. A. Kirillova, T. R. Yeazel, D. Asheghali, S. R. Petersen, S. Dort, K. Gall, M. L. Becker, Fabrication of biomedical scaffolds using biodegradable polymers. *Chem. Rev.* **121**, 11238–11304 (2021).
23. A. P. Raman, W. Li, S. Fan, Generating light from darkness. *Joule* **3**, 2679–2686 (2019).
24. Z. Xia, Z. Zhang, Z. Meng, L. Ding, Z. Yu, Thermoelectric generator using space cold source. *ACS Appl. Mater. Interfaces* **11**, 33941–33945 (2019).
25. S. Zhang, Z. Wu, Z. Liu, E. Mu, Y. Liu, Y. Lv, T. Thundat, Z. Hu, Power generation on chips: Harvesting energy from the sun and cold space. *Adv. Mater. Technol.* , 2200478 (2022).
26. S. Ishii, T. D. Dao, T. Nagao, Radiative cooling for continuous thermoelectric power generation in day and night. *Appl. Phys. Lett.* **117**, 013901 (2020).
27. S. Y. Heo, D. H. Kim, Y. M. Song, G. J. Lee, Determining the effectiveness of radiative cooler-integrated solar cells. *Adv. Energy Mater.* **12**, 2103258 (2022).
28. S. I. Jeong, B. S. Kim, Y. M. Lee, K. J. Ihn, S. H. Kim, Y. H. Kim, Morphology of elastic poly(L-lactide-co-ε-caprolactone) copolymers and in vitro and in vivo degradation behavior of their scaffolds. *Biomacromolecules* **5**, 1303–1309 (2004).
29. L. Yin, H. Cheng, S. Mao, R. Haasch, Y. Liu, X. Xie, S. W. Hwang, H. Jain, S. K. Kang, Y. Su, R. Li, Y. Huang, J. A. Rogers, Dissolvable metals for transient electronics. *Adv. Funct. Mater.* **24**, 645–658 (2014).
30. V. R. Feig, H. Tran, Z. Bao, Biodegradable polymeric materials in degradable electronic devices. *ACS Cent. Sci.* **4**, 337–348 (2018).
31. S. Pradhan, V. K. Yadavalli, Photolithographically printed flexible silk/PEDOT:PSS temperature sensors. *ACS Appl. Electron. Mater.* **3**, 21–29 (2021).
32. A. G. Kanani, S. H. Bahrami, Effect of changing solvents on poly(ε-caprolactone) nanofibrous webs morphology. *J. Nanomater.* **2011**, 724153 (2011).
33. L. Xu, K. Crawford, C. B. Gorman, Effects of temperature and pH on the degradation of poly(lactic acid) brushes. *Macromolecules* **44**, 4777–4782 (2011).
34. D. Li, X. Liu, W. Li, Z. Lin, B. Zhu, Z. Li, J. Li, B. Li, S. Fan, J. Xie, J. Zhu, Scalable and hierarchically designed polymer film as a selective thermal emitter for high-performance all-day radiative cooling. *Nat. Nanotechnol.* **16**, 153–158 (2021).
35. X. Yin, R. Yang, G. Tan, S. Fan, Terrestrial radiative cooling: Using the cold universe as a renewable and sustainable energy source. *Science* **370**, 786–791 (2020).
36. K. Tang, K. Dong, J. Li, M. P. Gordon, F. G. Reichertz, H. Kim, Y. Rho, Q. Wang, C. Y. Lin, C. P. Grigoropoulos, A. Javey, J. J. Urban, J. Yao, R. Levinson, J. Wu, Temperature-adaptive radiative coating for all-season household thermal regulation. *Science* **374**, 1504–1509 (2021).
37. R. E. Hummel, *Electronic Properties of Materials* (Springer, ed. 4, 2011).
38. K. Nan, S. D. Kang, K. Li, K. J. Yu, F. Zhu, J. Wang, A. C. Dunn, C. Zhou, Z. Xie, M. T. Agne, H. Wang, H. Luan, Y. Zhang, Y. Huang, G. J. Snyder, J. A. Rogers, Compliant and stretchable thermoelectric coils for energy harvesting in miniature flexible devices. *Sci. Adv.* **4**, eaau5849 (2018).
39. H. You, Z. Li, Y. Shao, X. Yuan, W. Liu, H. Tang, Q. Zhang, Y. Yan, X. Tang, Flexible Bi_2Te_3-based thermoelectric generator with an ultra-high power density. *Appl. Therm. Eng.* **202**, 117818 (2022).
40. B. Lee, H. Cho, K. T. Park, J. S. Kim, M. Park, H. Kim, Y. Hong, S. Chung, High-performance compliant thermoelectric generators with magnetically self-assembled soft heat conductors for self-powered wearable electronics. *Nat. Commun.* **11**, 5948 (2020).
41. T. Sun, B. Zhou, Q. Zheng, L. Wang, W. Jiang, G. J. Snyder, Stretchable fabric generates electric power from woven thermoelectric fibers. *Nat. Commun.* **11**, 572 (2020).
42. A. I. Hochbaum, R. Chen, R. D. Delgado, W. Liang, E. C. Garnett, M. Najarian, A. Majumdar, P. Yang, Enhanced thermoelectric performance of rough silicon nanowires. *Nature* **451**, 163–167 (2008).

43. S. Elyamny, E. Dimaggio, S. Magagna, D. Narducci, G. Pennelli, High power thermoelectric generator based on vertical silicon nanowires. *Nano Lett.* **20**, 4748–4753 (2020).
44. E. Mu, Z. Wu, Z. Wu, X. Chen, Y. Liu, X. Fu, Z. Hu, A novel self-powering ultrathin TEG device based on micro/nano emitter for radiative cooling. *Nano Energy* **55**, 494–500 (2019).
45. Z. Chen, L. Zhu, W. Li, S. Fan, Simultaneously and synergistically harvest energy from the sun and outer space. *Joule* **3**, 101–110 (2019).
46. Z. Xia, Z. Zhang, Z. Meng, Z. Yu, A 24-hour thermoelectric generator simultaneous using solar heat energy and space cold energy. *J. Quant. Spectrosc. Radiat. Transf.* **251**, 107038 (2020).
47. L. Fan, W. Li, W. Jin, M. Orenstein, S. Fan, Maximal nighttime electrical power generation via optimal radiative cooling. *Opt. Express* **28**, 25460–25470 (2020).
48. W. Ren, Y. Sun, D. Zhao, A. Aili, S. Zhang, C. Shi, J. Zhang, H. Geng, J. Zhang, L. Zhang, J. Xiao, R. Yang, High-performance wearable thermoelectric generator with self-healing, recycling, and Lego-like reconfiguring capabilities. *Sci. Adv.* **7**, eabe0586 (2021).
49. S. Ishii, A. Miura, T. Nagao, K. I. Uchida, Simultaneous harvesting of radiative cooling and solar heating for transverse thermoelectric generation. *Sci. Technol. Adv. Mater.* **22**, 441–448 (2021).
50. K. Gao, J. Yang, H. Shen, Y. Liu, Y. Li, M. Zhang, Uninterrupted self-generation thermoelectric power device based on the radiative cooling emitter and solar selective absorber. *Sol. RRL* **6**, 2100975 (2022).
51. S.-H. Byun, J. H. Yun, S.-Y. Heo, C. Shi, G. J. Lee, K.-C. Agno, K.-I. Jang, J. Xiao, Y. M. Song, J.-W. Jeong, Self-cooling gallium-based transformative electronics with a radiative cooler for reliable stiffness tuning in outdoor use. *Adv. Sci.* **9**, 2202549 (2022).
52. H. Zhang, K. C. S. Ly, X. Liu, Z. Chen, M. Yan, Z. Wu, X. Wang, Y. Zheng, H. Zhou, T. Fan, Biologically inspired flexible photonic films for efficient passive radiative cooling. *Proc. Natl. Acad. Sci. U.S.A.* **117**, 14657–14666 (2020).
53. M. Li, M. Zhang, F. K. Mahar, L. Wei, Z. Wang, X. Wang, K. Wei, Fabrication of fibrous nanofiber membranes for passive radiation cooling. *J. Mater. Sci.* **57**, 16080–16090 (2022).
54. X. Cai, Y. Wang, Y. Luo, J. Xu, L. Zhao, Y. Lin, Y. Ning, J. Wang, L. Gao, D. Li, Rationally tuning phase separation in polymeric membranes toward optimized all-day passive radiative coolers. *ACS Appl. Mater. Interfaces* **14**, 27222–27232 (2022).
55. H. Sun, F. Tang, Q. Chen, L. Xia, C. Guo, H. Liu, X. Zhao, D. Zhao, L. Huang, J. Li, L. Chen, A recyclable, up-scalable and eco-friendly radiative cooling material for all-day sub-ambient comfort. *Chem. Eng. J.* , 139786 (2023).
56. C. Park, C. Park, X. Nie, J. Lee, Y. S. Kim, Y. Yoo, Fully organic and flexible biodegradable emitter for global energy-free cooling applications. *ACS Sustain. Chem. Eng.* **10**, 7091–7099 (2022).
57. X. Liu, M. Zhang, Y. Hou, Y. Pan, C. Liu, C. Shen, Hierarchically superhydrophobic stereocomplex poly (lactic acid) aerogel for daytime radiative cooling. *Adv. Funct. Mater.* **32**, 2207414 (2022).

Acknowledgments

Funding: This work was supported by a Korea University grant, the KU-KIST Graduate School of Converging Science and Technology Program, National Research Foundation of Korea (NRF) grants funded by the Korean government (the Ministry of Science, ICT, MSIT) (grants NRF-2018M3D1A1058997 and RS-2022-00165524), the Nano-Material Technology Development Program through the National Research Foundation of Korea (NRF) funded by the Ministry of Science and ICT (NRF-2021R1A4A2001827, NRF-2021M3H4A1A04086552, NRF-2022M3H4A1A02046445, and NRF-2022M3C1A3081312), an Institute for Information and Communications Technology Planning and Evaluation (IITP) grant funded by the Korean government (MSIT) [no. 2019-0-01842, Artificial Intelligence Graduate School Program (GIST)], a Korea Medical Device Development Fund Grant funded by the Korean government (the Ministry of Science and ICT; the Ministry of Trade, Industry, and Energy; the Ministry of Health and Welfare; and the Ministry of Food and Drug Safety) (1711174536 and RS-2020-KD000138), and the Ministry of the Science and ICT (MSIT) under the ICT Creative Consilience program (IITP-2023-2020-0-01819) supervised by the IITP. **Author contributions:** W.B.H., S.-Y.H., Y.M.S., and S.-W.H. conceived and designed the research. W.B.H., S.-Y.H., D.K., and S.M.Y. performed the experiments. S.M.Y., G.-J.K., G.J.L., D.-J.K., K.R., J.H.L., J.-W.S., T.-M.J., S.H., H.K., J.H.L., and D.H.K. contributed to the fabrication and characterization of devices. S.H.K. supported the experiments and commented on the paper. W.B.H., S.-Y.H., D.K., Y.M.S., and S.-W.H. co-wrote the manuscript. **Competing interests:** The authors declare that they have no competing interests. **Data and materials availability:** All data needed to evaluate the conclusions in the paper are present in the paper and/or the Supplementary Materials.

Submitted 1 November 2022
Accepted 5 January 2023
Published 1 February 2023
10.1126/sciadv.adf5883